Available online at www.sciencedirect.com
SCIENCE DIRECT
Thin Solid Films 510 (2006) 339 – 345
thin solid films
www.elsevier.com/locate/tsf

Orientation-dependent mobilities from analyses of two-dimensional TiN(111) island decay kinetics

J. Bareño [a,*], S. Kodambaka [a], S.V. Khare [b], W. Święch [a], I. Petrov [a], J.E. Greene [a]

[a] Department of Materials Science and the Frederick Seitz Materials Research Laboratory, University of Illinois, 104 South Goodwin Avenue, Urbana, IL 61801, USA
[b] Department of Physics and Astronomy, The University of Toledo, 2801 West Bancroft Street, Toledo, OH 43606, USA

Received 30 May 2005; received in revised form 24 October 2005; accepted 12 December 2005
Available online 24 January 2006

Abstract

We present a method for the determination of orientation-dependent mobilities $\Gamma_{\mathrm{eff}}(\varphi)$ based upon analyses of the detachment-limited coarsening/decay kinetics of equilibrium-shaped two-dimensional islands. An exact analytical expression relating the orientation-dependence of $\Gamma_{\mathrm{eff}}(\varphi)$ to that of the anisotropic step energies $\beta(\varphi)$ is derived. This provides relative values of $\Gamma_{\mathrm{eff}}(\varphi)$ to within an orientation-independent scale factor that is proportional to the decay rate of the island area. Using in situ high temperature (T=1550–1700 K) low-energy electron microscopy measurements of two-dimensional TiN island coarsening/decay kinetics on TiN(111) terraces for which $\beta(\varphi)$ values are known [Phys. Rev. B 67 (2003) 35409], we demonstrate the applicability of our analytic formulation for the determination of absolute $\Gamma_{\mathrm{eff}}(\varphi)$ values.

Keywords: Surface diffusion; Surface thermodynamics; Models of surface kinetics; Low-energy electron microscopy

1. Introduction

NaCl-structure TiN and related transition-metal (TM) nitrides are widely used as hard wear-resistant coatings on cutting tools, diffusion-barriers in microelectronic devices, corrosion-resistant layers on mechanical components, and abrasion-resistant thin films on optics and architectural glass. Controlling the microstructural and surface morphological evolution of polycrystalline TM nitride films is important in all of these applications. This fact has spurred interest in modeling polycrystalline TM nitride thin film growth [1], a complex phenomenon controlled by the interplay of thermodynamic driving forces and kinetic limitations, as a function of deposition conditions. Developing a quantitative model, however, requires knowledge of atomic-level processes, site-specific surface energetics, and rate-limiting mechanisms. Recently, considerable progress has been made toward the determination of absolute orientation-dependent step energies, step stiffnesses, and kink energies [2,3], as well as identifying the mechanisms controlling the kinetics of two-dimensional (2D) TiN island coarsening/decay (Ostwald ripening) [4,5] and island shape equilibration on (001) and (111) TiN terraces [6–8]. Here, we focus on the extraction of anisotropic attachment/detachment mobilities from analyses of 2D TiN(111) island coarsening/decay kinetics.

Ostwald ripening is a phenomenon in which larger islands grow at the expense of smaller ones and, for the particular case of isotropic (i.e. circular) islands, is described by the classical Gibbs–Thomson equation [4,5]

$$\rho^{\mathrm{eq}} = \rho_{\infty}^{\mathrm{eq}} \exp\left(\frac{\Omega\beta}{kTr_{\mathrm{c}}}\right), \tag{1}$$

where ρ^{eq} is the equilibrium free adatom concentration associated with an island of radius r_{c}, $\rho_{\infty}^{\mathrm{eq}}$ is the equilibrium free adatom concentration of a straight step, β is the isotropic step energy per unit step length, and Ω is the unit atomic area. The process of coarsening is simply curvature-driven mass transport. Smaller islands have higher curvature, and hence higher adatom concentration than larger islands; this results in adatom transfer from small to large islands.

Experimental coarsening studies have mostly been carried out on isotropic, or near-isotropic, surfaces such as Ag(111)

* Corresponding author. ESB 1-129, 1101 W. Springfield Avenue, Urbana, IL 61801 USA. Tel.: +1 217 3337080; fax: +1 217 2441638.
E-mail address: bareno@uiuc.edu (J. Bareño).

0040-6090/$ - see front matter © 2005 Elsevier B.V. All rights reserved.
doi:10.1016/j.tsf.2005.12.164

[9,10], Cu(111) [11], Cu(001) [12], and TiN(001) [7], and modeled based upon isotropic adatom transport. The reconstructed Si(001) 2×1 surface, although anisotropic in nature, exhibits isotropic coarsening/decay kinetics [13]. On isotropic metal surfaces, novel adatom transport phenomena, such as fast interlayer mass transport across small terraces (a few atomic spacings wide) and the self selection of an optimal mound slope during decay, have been observed and explained based upon the absence of preferred sites for interlayer transport [14], the interplay between electronic occupation and the Ehrlich barrier [15,16], and two-atom interlayer-exchange processes [17]. Deviation from isotropic coarsening/decay kinetics has, so far, only been reported for Au(110) [18–21], Ag(110) [22,23], and TiN(111) [6]. In the case of Au(110), a missing-row reconstruction leads to an anomalous Au(110) island decay behavior, while anisotropic Ag(110) and TiN(111) island decay kinetics were attributed to orientation-dependent attachment/detachment barriers. Yao et al. [24] derived general analytic expressions and scaling relations for the decay of 2D islands on highly anisotropic surfaces, where both surface diffusivities and attachment/detachment rates may be anisotropic. Orientation-dependent effective attachment/detachment mobilities Γ have been measured for Ag(110) [25] and Si(001) [13]. Since the differences found between the absolute Γ values for different step orientations were smaller than the experimental uncertainties, the authors concluded that Γ is isotropic with no orientation-dependence on both Ag(110) and Si(001) surfaces.

In the following section, we develop a theoretical approach for determining orientation-dependent mobilities $\Gamma_{\mathrm{eff}}(\varphi)$ from analyses of 2D anisotropic island coarsening/decay kinetics in the detachment-limited regime [26]. An exact analytical expression relating $\Gamma_{\mathrm{eff}}(\varphi)$ to the anisotropic step energies $\beta(\varphi)$ is derived, showing that $\Gamma_{\mathrm{eff}}(\varphi)$ and $\beta(\varphi)$ exhibit *exactly the same* orientation-dependence. Thus if absolute values of $\beta(\varphi)$ are known, e.g. from step fluctuation experiments [3], then absolute values of $\Gamma_{\mathrm{eff}}(\varphi)$ can be obtained.

Next, we demonstrate the applicability of our analytic formulation using in situ high temperature (T=1550–1700 K) low-energy electron microscopy (LEEM) [27] measurements of 2D TiN island coarsening/decay kinetics to determine $\Gamma_{\mathrm{eff}}(\varphi)$ on TiN(111) terraces. Our approach is valid under the condition that islands maintain their equilibrium shape during coarsening/decay via detachment-limited kinetics.

2. Theory

In this section, we demonstrate that the effective mobility $\Gamma_{\mathrm{eff}}(\varphi)$ of a 2D island undergoing a detachment-limited coarsening process, while preserving its equilibrium shape, has the same dependency on the step orientation φ as the experimentally accessible quantities $v_{\mathrm{n}}(\varphi)$, the orientation-dependent velocity normal to the island edge, and $\beta(\varphi)$, the island step energy per unit length. Then, we derive an exact analytical expression relating $\beta(\varphi)$ to $\Gamma_{\mathrm{eff}}(\varphi)$, thereby providing a means for determining absolute $\Gamma_{\mathrm{eff}}(\varphi)$ values for 2D islands from measurements of their orientation-dependent $\beta(\varphi)$ values and decay rate $\mathrm{d}A/\mathrm{d}t$ during annealing.

The decay of an arbitrary-shaped 2D island can be described in cylindrical polar coordinates by specifying the rate of change of the distance between the island center of mass and its edge, $r\equiv r(\theta,t)$, as a function of the polar angle θ and time t. In the case of detachment-limited decay kinetics, for which adatom diffusion through the terrace is sufficiently fast to consider the adatom concentration near the island edge to be in steady state, the normal velocity v_{n} of the island edge is [6,26]

$$v_{\mathrm{n}}(\varphi,t) = -\Gamma(\varphi)\Omega\left[\frac{\rho^{\mathrm{eq}}(\varphi,t)}{\rho_{\infty}^{\mathrm{eq}}}-1\right]+D^{\mathrm{edge}}\nabla^2\mu, \tag{2}$$

where D^{edge} is the orientation-dependant edge diffusion coefficient, Γ is the attachment-detachment mobility, and φ is the local normal to the step, defined as

$$\varphi=\theta-\arctan(r'/r). \tag{3}$$

The superscript prime denotes a derivative with respect to θ.

There are two limiting cases for which the second term in Eq. (2) can be neglected. One is when the edge diffusion is so slow that $D^{\mathrm{edge}}\nabla^2\mu \ll \Gamma(\varphi)\Omega\left[\frac{\rho^{\mathrm{eq}}(\varphi,t)}{\rho_{\infty}^{\mathrm{eq}}}-1\right]$, the other is when the edge diffusion is so fast that the island is in equilibrium (μ=constant) on the timescale of data acquisition. This latter condition is usually satisfied at high temperatures, when diffusion along the island edge is much faster than detachment of adatoms to the terrace. In this case, adatom detachment is the rate-limiting process governing the observed island coarsening, and the step mobility Γ entering Eq. (2) is an effective mobility Γ_{eff} that includes contributions from both edge diffusion and attachment/detachment barriers.

In Eq. (2), $\rho^{\mathrm{eq}}(\varphi,t)$ and $\rho_{\infty}^{\mathrm{eq}}$ are related through the Gibbs–Thomson equation which, for arbitrary island shapes, can be expressed as [2]

$$\rho^{\mathrm{eq}}=\rho_{\infty}^{\mathrm{eq}}\exp\left(\frac{\tilde{\beta}(\varphi)\kappa(\theta)\Omega}{kT}\right), \tag{4}$$

where $\tilde{\beta}(\varphi)\equiv\beta(\varphi)+[d^2\beta(\varphi)/d\varphi^2]$ is the step stiffness, and $\kappa(\theta,t)=\left(\left(r^2+2(r')^2-rr''\right)/\left(r^2+(r')^2\right)^{3/2}\right)$ is the local step curvature [28]. Following Refs. [29] and [30], we combine Eqs. (2) and (4), expand the exponential in Eq. (4) to first order [31], and obtain

$$v_n(\varphi,t) = -\left[\frac{\Omega^2}{kT}\right]\Gamma_{\mathrm{eff}}(\varphi)\tilde{\beta}(\varphi)\kappa(\theta,t). \tag{5}$$

The rate of change $\mathrm{d}A(t)/\mathrm{d}t$ of a 2D anisotropic island area in the detachment-limited regime is related to $v_{\mathrm{n}}(\varphi,t)$ through the expression

$$\begin{aligned}\frac{dA}{dt}(t) &= \int_0^{2\pi} v_n(\varphi,t)\sqrt{r^2(\theta,t)+(r'(\theta,t))^2}\,d\theta\\ &= -\left[\frac{\Omega^2}{kT}\right]\int_0^{2\pi}\Gamma_{\mathrm{eff}}(\varphi)\tilde{\beta}(\varphi)d\varphi.\end{aligned} \tag{6}$$

In deriving Eq. (6), we have substituted $d\theta=d\varphi/(\kappa(\theta)\sqrt{r^2(\theta,t)+(r'(\theta,t))^2})$, which is obtained from Eq. (3). The right side of Eq. (6) does not depend on time. Thus, the area of

an anisotropic island decreases, in the detachment-limited regime, at a constant rate that is proportional to the product of the orientation-averaged detachment rate and step stiffness.

For any equilibrium-shaped island, the product $\tilde{\beta}(\varphi)\kappa(\theta,t)$ is independent of step orientation and depends only on the island size [2]. From Ref. [2], $\tilde{\beta}(\varphi)\kappa(\theta,t)$ can be expressed in terms of an average island radius $R_{\mathrm{avg}}(t) \equiv (A(t)/\pi)^{1/2}$ as $B/R_{\mathrm{avg}}(t)$, where B is an orientation-independent constant which sets the energy scale of the equilibrium island chemical potential. Expressing Eq. (5) in terms of B yields

$$v_n(\varphi,t) = -\left[\frac{B\Omega^2}{kTR_{\mathrm{avg}}(t)}\right]\Gamma_{\mathrm{eff}}(\varphi). \tag{7}$$

From Eq. (7), we observe that the normal velocity of the edge of an island that maintains its equilibrium shape during coarsening/decay has the *same* orientation dependence as that of the attachment/detachment rate. In the following paragraphs, we focus on relating $v_{\mathrm{n}}(\varphi,t)$ to $\beta(\varphi)$.

The kinematic expression for $v_{\mathrm{n}}(\varphi,t)$ is

$$v_n(\varphi,t) \equiv \left(\dot{r}(\theta,t)\hat{r} + r(\theta,t)\dot{\theta}\hat{\theta}\right)\cdot\frac{r(\theta,t)\hat{r} - r'(\theta,t)\hat{\theta}}{\sqrt{r^2(\theta,t)+(r'(\theta,t))^2}}$$

$$= \frac{r(\theta,t)\dot{r}(\theta,t)}{\sqrt{r^2(\theta,t)+(r'(\theta,t))^2}}, \tag{8}$$

where the dot superscript denotes a derivative with respect to time t, and $\hat{r}$ and $\hat{\theta}$ are the radial and azimuthal unit vectors, respectively. In deriving Eq. (8), we assume that the islands are stationary, i.e. $\dot{\theta}=0$. For an island that maintains its equilibrium shape during the coarsening process, $\dot{r}(\theta,t)/r(\theta,t)$ does not depend on θ and is only a function of t. Hence, the time-dependent island boundary can be represented in terms of a non-dimensional equilibrium shape function $s(\theta)$ as

$$r(\theta,t) = R_{\mathrm{avg}}(t)\cdot s(\theta), \tag{9}$$

in which $s(\theta)$ is related to $\beta(\varphi)$ as [32]

$$\frac{\beta(\varphi)}{B} = \frac{s^2(\theta)}{\sqrt{s^2(\theta)+(s'(\theta))^2}}. \tag{10}$$

It is important to note that B determines the energy scale of the surface equilibrium chemical potential; for circular islands, $B=\beta$ and $R_{\mathrm{avg}}=r$. The equation $\beta(\varphi)/R(\theta)=$constant (often referred to as the "Wulff relation") is *not* valid for any arbitrary step orientation φ [32]. This relationship is *only* valid at the orientations corresponding to maxima or minima in β, i.e. $s(\theta)=0$, as can be seen from Eq. (10).

Combining Eqs. (8)–(10), eliminating $s(\theta)$, and using $\frac{\mathrm{d}A(t)}{\mathrm{d}t} = 2\pi R_{\mathrm{av}}(t)\frac{dR_{\mathrm{av}}(t)}{dt}$ yields

$$v_n(\varphi,t) = \left[\frac{dA(t)/dt}{2\pi BR_{\mathrm{avg}}(t)}\right]\beta(\varphi). \tag{11}$$

We note that Eq. (11) has been derived without invoking the constraint of detachment-limited kinetics. This equation provides a means to separate the time- and orientation-dependent components of v_{n} and is valid for any island that maintains its equilibrium shape during decay, independently of the decay and shape-preservation mechanisms. In the case of diffusion-limited decay, for example, v_{n} is proportional to the gradient of the adatom concentration normal to the island edge [26], which is in turn proportional to $\beta(\varphi)$. In the detachment-limited regime, however, $\mathrm{d}A/\mathrm{d}t$ is independent of island size, as shown by Eq. (6). Therefore, the product $v_{\mathrm{n}}(\varphi,t)R_{\mathrm{avg}}(t)$ is constant, independent of both time t and island size R_{avg}.

Setting Eqs. (7) and (11) equal, we obtain the result that

$$\Gamma_{\mathrm{eff}}(\varphi) = \left[\frac{-kT}{2\pi\Omega^2B^2}\frac{dA(t)}{dt}\right]\beta(\varphi), \tag{12}$$

where the negative sign arises from the fact that $\mathrm{d}A/\mathrm{d}t<0$ during island decay. Eqs. (11) and (12) show that $\Gamma_{\mathrm{eff}}(\varphi)$ has the same dependency on the step orientation φ as the experimentally accessible quantities $v_{\mathrm{n}}(\varphi,t)$ and $\beta(\varphi)$. In the following sections, we apply this formulation to determine $\Gamma_{\mathrm{eff}}(\varphi)$ for 2D islands on TiN(111).

3. Experimental procedure

Epitaxial TiN(111) layers, 2000 Å thick, were grown on polished $Al_2O_3(0001)$ substrates (0.5 mm thick × 9 mm diameter) at a temperature $T_s=1050$ K in a load-locked multichamber ultra-high vacuum (UHV) system using magnetically unbalanced dc magnetron sputter deposition [33] following the procedure described in Ref. [2]. The TiN(111) samples were then transferred to a UHV multichamber LEEM system [34], with a base pressure of 2×10^{-10} Torr, which is equipped with facilities for residual gas analysis, electron-beam evaporation, ion sputtering, Auger electron spectroscopy (AES), and low-energy electron diffraction (LEED). Sample temperatures were measured by optical pyrometry and calibrated using temperature-dependent TiN emissivity data obtained by spectroscopic ellipsometry. The TiN(111) layers were degassed in the LEEM sample preparation chamber at 1073 K for approximately 2 h. This procedure results in sharp 1 × 1 LEED patterns with a 3-fold symmetry, as expected for bulk-terminated TiN(111) [3]. In situ AES analyses indicate that the samples contain ≃2 mol% oxygen, most likely in the form of TiO which is isostructural [35] and mutually soluble with TiN.

Homoepitaxial TiN(111) overlayers, 50–200 Å thick, were deposited at 1023 K by reactive evaporation from Ti rods (99.999% purity) at a rate of ≃0.02 ML/s and annealed for 2–3 days in 5×10^{-8} Torr N_2 (99.999%) at temperatures $T>1200$ K. These deposition/annealing cycles were repeated until large (>1000 Å) atomically smooth TiN(111) terraces and 3D mounds, consisting of concentrically stacked 2D TiN islands, are obtained.

Bright-field (BF) LEEM images documenting the coarsening/decay of these island stacks, in which average island areas range from 2×10^{-2} to 13×10^{-2} μm^2, were acquired at a video rate of 30 frames/s as a function of annealing time t and temperature T (see Fig. 1a, for example). Pixel resolution

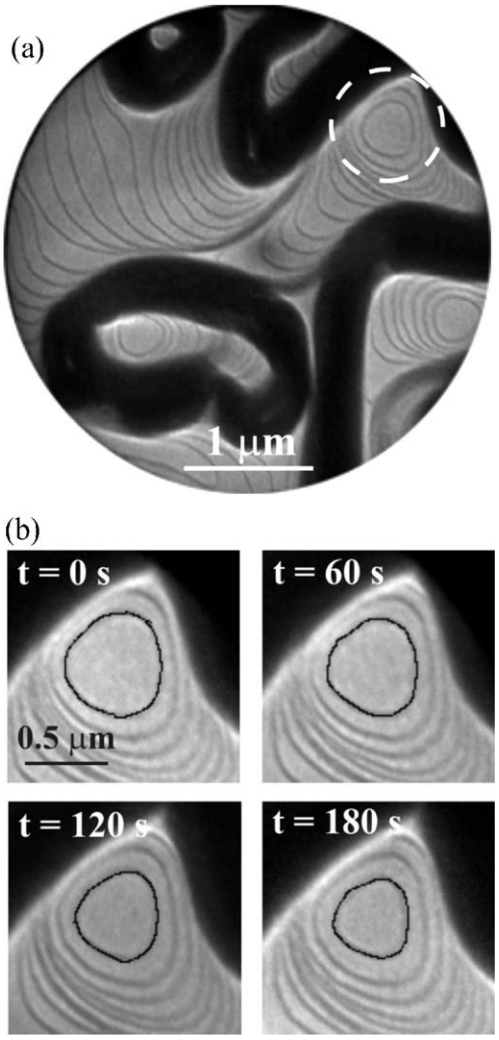

Fig. 1. (a) Typical BF-LEEM image (field of view=4 μm) of a TiN(111) surface during annealing at 1559 K. (b) Higher-resolution images (fields of view=1.1 μm) of the highlighted region in (a) at annealing times 0, 60, 120, and 180 s. The boundary of the upper island is outlined. All images are part of a video file obtained at 30 frames per second.

corresponding to a 4 μm field of view is ≃85 Å. Typical electron probe beam energies were 5 to 25 eV. The samples were allowed to thermally stabilize at each temperature for 10 to 15 s prior to acquiring LEEM videos. From each measurement sequence, time-dependent island boundaries $r(\theta,t)$ and areas $A(t)$ were determined using Image SXM, an image processing software [36].

4. Results and discussion

Fig. 1a shows a typical BF-LEEM image (field of view=4.0 μm) of the surface morphology of a TiN(111) sample acquired during annealing, in this case at $T=1559$ K. The thick dark lines are ≃300 Å deep grooves bounding single-crystalline TiN(111) domains oriented 180° with respect to each other due to the three-fold symmetry of the TiN(111) surface [37]. Within these domains, we observe bilayer-height TiN(111) steps [38] (thin lines) and stacks of 2D islands with truncated-hexagonal shapes bounded by alternating long and short ⟨110⟩ steps [3]. Fig. 1b shows higher magnification images (field of view= 1.1 μm) of the island stack highlighted by the white dashed circle in Fig. 1a. These images were acquired at times $t=0$, 60, 120, and 180 s, where we define $t=0$ as the time at which the first image in any given sequence is acquired. During annealing, we follow the decay of the upper island in the stack (highlighted in Fig. 1b), which retains its truncated-hexagonal shape during the process, in agreement with our previously published STM results [6,39].

Fig. 2 is a plot of the area A of the upper island in Fig. 1b vs. annealing time t. We find that A decreases linearly with time at a rate $dA/dt=-(435\pm4)\times10^2$ Å^2 s^{-1}. A constant decay rate is the signature of detachment-limited decay kinetics described by Eq. (6). This behavior, linear decay while preserving a constant equilibrium shape, is typical of LEEM data obtained from over 50 islands at temperatures ranging from 1550 to 1700 K [37].

In order to avoid the tedious process of numerically computing $v_n(\varphi,t)$ from discrete $r(\theta,t)$ data, we fit the island shape with a function of the form

$$r(\theta,t)=a(t)\cdot f(\theta,t)$$

$$f(\theta,t)=1+b(t)\cdot\cos(3\theta+\theta_0), \tag{13}$$

where θ_0 is a constant. This is the simplest function consistent with the threefold symmetry of the TiN(111) surface, and allows us to calculate $v_n(\varphi,t)$ analytically from Eq. (8).

Figs. 3a and b are typical Cartesian and polar plots, respectively, of experimentally measured (open circles) r versus θ data for the island shown in Fig. 1b, fit with Eq. (13) (solid lines). As an additional check that the island maintains a constant shape during the decay process, we used Eq. (13) (fits to the data in Fig. 3) to calculate the parameter χ, a measure of the island shape anisotropy, defined as

$$\chi(t)\equiv\frac{r_{\min}(t)}{r_{\max}(t)}=\frac{1-b(t)}{1+b(t)}. \tag{14}$$

In Eq. (14), $r_{\min}$ and $r_{\max}$ are, respectively, the minimum and maximum radial distances from the center of a TiN(111) island to its edge, i.e. to the center of the <110> steps designated as S_1 and S_2 (see Fig. 3), and $b(t)$ is defined in Eq. (13).

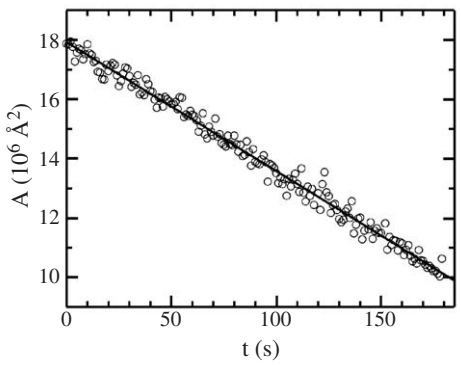

Fig. 2. Measured (open circles) island areas A vs. annealing time t for the 2D TiN(111) adatom island outlined in Fig. 1b. The solid line is a least squares fit to the data.

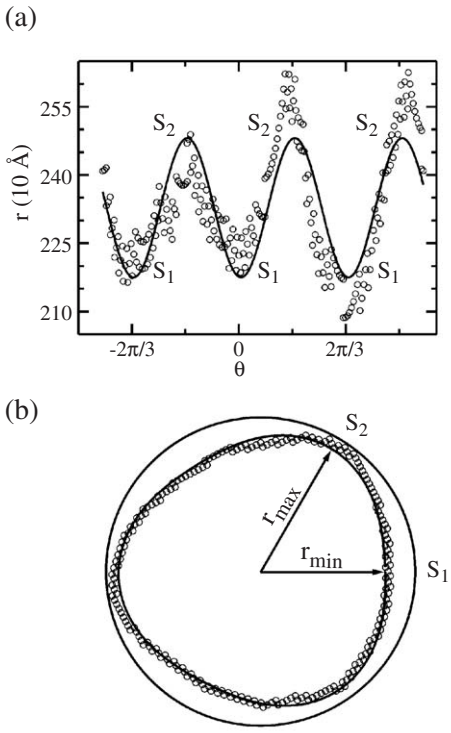

Fig. 3. (a) Cartesian and (b) polar plots of r vs. θ for the TiN(111) island outlined in Fig. 1b. Open circles represent experimental data while the solid lines are fit using Eq. (13). The two <110> steps are labeled S_1 and S_2 and the corresponding radial distances from the center of the island are r_{min} and r_{max}, respectively.

Fig. 4 is a plot of χ versus annealing time for the TiN(111) island shown in Fig. 1b. We find that $\chi(t)$ remains constant at $\chi = 0.87 \pm 0.02$ (solid line in Fig. 4), indicating that the island shape remains constant during the coarsening process [40]; i.e. $db/dt = 0$, as required in the derivation of Eqs. (7) and (12) in Section 2. The apparent island anisotropy variation with t is due to increasing experimental uncertainties in island boundary measurement for smaller islands. In the following paragraphs, we focus on providing experimental evidence for the validity of Eqs. (7), (11), and (12), and then we use the equations to obtain

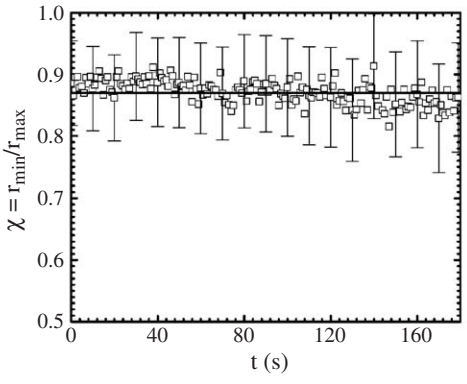

Fig. 4. A plot of the anisotropy parameter $\chi(t) = [r_{min}(t)/r_{max}(t)]$ vs. time t for the 2D TiN(111) island outlined in Fig. 1b during annealing at $T = 1559$ K. The solid line is the average $\chi(t)$ value. The vertical scale of the plot ranges from the value corresponding to an island with the shape of an equilateral triangle ($\chi = 0.5$) to that corresponding to an isotropic circular island ($\chi = 1$). Error bars are shown only for a subset of 20 data points to improve figure clarity.

absolute $\Gamma_{eff}(\varphi)$ values for 2D TiN(111) islands as a function of orientation φ.

Eq. (12) was derived by relating Eqs. (7) and (11) through the step velocity $v_n(\varphi, t)$ or, equivalently, through the product $P(\varphi) \equiv R_{avg}(t) v_n(\varphi, t)$. Substituting Eqs. (8) and (13) into $P(\varphi)$ and taking into account that $db/dt = 0$ for shape-preserving island decay, we obtain

$$P(\varphi) = R_{avg}(t) v_n(\varphi, t) = \frac{3\pi}{4} \frac{a(t)\dot{a}(t)(2 + b(t))(1 + b(t)\cos(3\theta + \theta_0))^2}{\sqrt{(1 + b(t)\cos(3\theta + \theta_0))^2 + (3b(t)\sin(3\theta + \theta_0))^2}}. \quad (15)$$

Eq. (7) predicts that $P(\varphi)$ is proportional to $\Gamma_{eff}(\varphi)$, and thus time-independent. Eq. (11) shows, in turn, that $P(\varphi)$ is also proportional to both dA/dt and $\beta(\varphi)$. Since $\beta(\varphi)$ has the same threefold symmetry as the experimental island shape [28] and dA/dt is constant for detachment-limited decay kinetics, $P(\varphi)$ is a time-independent function of φ, corresponding to the equilibrium island shape. Fig. 5 is a plot of the product $P(\varphi) \equiv R_{avg}(t) v_n(\varphi, t)$ calculated using Eq. (15) and the values for $a(t)$, $b(t)$, and θ_0 obtained from fitting Eq. (13) to the experimental island shape at each of 177 time steps. For clarity, Fig. 5 shows only data sets calculated at 20 equally spaced times during the decay process. We note that the functional form of $P(\varphi)$ exhibits three-fold symmetry and that all data sets agree to within a maximum uncertainty of 3%, verifying that $P(\varphi)$ does not depend on time. Thus, the results in Fig. 5 provide confirmation of the functional dependences of Eqs. (7) and (11).

To obtain *absolute* $\Gamma_{eff}(\varphi)$ values from $P(\varphi)$ using Eq. (7), we must first determine B. We do this by noting that the equilibrium island shape, described by Eqs. (10) and (13), fully determines the ratio $\beta(\varphi)/B$ [28]. Hence, the value of β at any particular orientation φ completely determines both $\beta(\varphi)$, at all φ values, and B. We obtain $\beta(S_2)$ for S_2 steps on TiN(111) by extrapolation of previously reported data [3] to $T = 1559$ K (the temperature used in the present experiment) through the expression [41,42]

$$\beta(T) = \beta(0) - \frac{kT}{a_{\parallel}} \left\{ 2\exp\left(\frac{-\varepsilon}{kT}\right) - \exp\left(\frac{-2\varepsilon}{kT}\right) \right\}. \quad (16)$$

$a_{\parallel}$ in Eq. (16) is the interplanar lattice spacing, 2.99 Å, parallel to the step edge; $\beta(0) = 0.34 \pm 0.07$ eV Å^{-1} [3] is the step

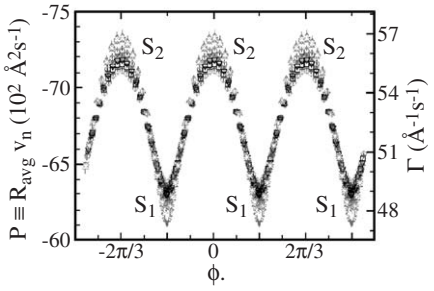

Fig. 5. A plot of $P(\varphi)$ [left vertical axis] and $\Gamma(\varphi)$ [right vertical axis] for the 2D TiN(111) island outlined in Fig. 1b. $P(\varphi) = R_{avg}(t) v_n(\varphi, t)$ while $\Gamma(\varphi)$ is the orientation-dependent attachment/detachment mobility.

energy at $T=0$ K; and $\varepsilon=0.14\pm0.02$ eV [3] is the kink formation energy of the step. Inserting these values yields $\beta(S_2)=0.31\pm0.08$ eV Å^{-1} at 1559 K.

From Eqs. (10) and (13), together with the average value for the island shape parameter $b=0.07\pm0.01$, we obtain $\beta(S_2)/B=1.07\pm0.02$. Thus, $B=0.29\pm0.08$ eV Å^{-1}. Substituting B, $\Omega=7.8$ Å^2 [43], and $kT=134\times10^{-3}$ eV, Eq. (7) can be written as $P(\varphi)\equiv R_{avg}(t)v_n(\varphi,t)=-C\Gamma_{eff}(\varphi)$, with $C=(129\pm35)$ Å^3. Finally, we substitute $P(\varphi)$ values from Fig. 5 and calculate absolute $\Gamma_{eff}(\varphi)$ values which range from 47 Å^{-1} s^{-1} for S_1 steps to 57 Å^{-1} s^{-1} for S_2 steps as plotted on the right vertical axis of Fig. 5.

As a self-consistency check, we also use Eq. (12) to calculate $\Gamma_{eff}(S_1)$ and $\Gamma_{eff}(S_2)$. Based upon the known value of $\beta(S_2)$ and the fact that $\beta(S_1)/\beta(S_2)\equiv r_{min}/r_{max}\equiv\chi$ [28], we obtain $\beta(S_1)=0.27\pm0.08$ eV Å^{-1}. Substituting values for B, $\beta(S_1)$, $\beta(S_2)$, Ω, and dA/dt into Eq. (12) yields $\Gamma_{eff}(S_1)=46\pm15$ Å^{-1} s^{-1} and $\Gamma_{eff}(S_2)=56\pm17$ Å^{-1} s^{-1} in good agreement with values determined from $P(\varphi)$ and Eq. (7).

Since we make no materials specific assumptions in the derivation of Eqs. (7), (11), and (12), we expect our method to be of general applicability to all materials systems. This allows orientation-dependant detachment mobilities to be obtained from analyses of detachment-limited coarsening/decay of anisotropic islands of arbitrary shape, provided that the equilibrium shape is maintained. This condition is usually satisfied at high temperatures when edge-atom diffusion is fast.

5. Conclusions

We have presented a method for the determination of orientation-dependent effective mobilities $\Gamma_{eff}(\varphi)$ from analyses of detachment-limited coarsening/decay kinetics of equilibrium-shaped two-dimensional islands. Initially, we show that island shape preservation during decay implies a link between the island step velocity $v_n(\varphi)$ and $\Gamma_{eff}(\varphi)$ through Eq. (7). Then we show that $v_n(\varphi)$ is proportional to the orientation-dependent step energy per unit length $\beta(\varphi)$ as expressed by Eq. (11). From these two results, we derived an exact analytical expression relating the orientation-dependence of $\Gamma_{eff}(\varphi)$ with that of $\beta(\varphi)$. This provides relative values of $\Gamma_{eff}(\varphi)$ to within an orientation-independent scale $\Gamma_{eff}(\varphi)$ ale factor that is proportional to the island decay rate. Using in situ high temperature LEEM, we apply this method to 2D TiN(111) islands, for which $\beta(\varphi)$ is known [3], by measuring island coarsening/decay kinetics at 1559 K. We obtain $\Gamma_{eff}(\varphi)$ values ranging from 46 ± 15 for S_1 steps to 56 ± 17 Å^{-1} s^{-1} for S_2 steps, as a function of orientation φ.

Acknowledgements

The authors gratefully acknowledge the financial support of the U.S. Department of Energy (DOE), Division of Materials Science, under Contract No. DEFG02-91ER45439 through the University of Illinois Frederick Seitz Materials Research Laboratory (FS-MRL). We also appreciate the use of the facilities in the Center for Microanalysis of Materials, partially supported by DOE, at the FS-MRL.

References

[1] F.H. Baumann, D.L. Chopp, T. Díaz de la Rubia, G.H. Gilmer, J.E. Greene, H. Huang, S. Kodambaka, P. O'Sullivan, I. Petrov, MRS Bull. 26 (2001) 182.
[2] S. Kodambaka, S.V. Khare, V. Petrova, A. Vailionis, I. Petrov, J.E. Greene, Surf. Sci. 513 (2002) 468.
[3] S. Kodambaka, S.V. Khare, V. Petrova, D.D. Johnson, I. Petrov, J.E. Greene, Phys. Rev., B 67 (2003) 035409.
[4] C. Herring, in: W.E. Kingston (Ed.), The Physics of Powder Metallurgy, McGraw-Hill, New York, 1951, p. 143.
[5] W.W. Mullins, Interface Sci. 9 (2001) 9.
[6] S. Kodambaka, V. Petrova, S.V. Khare, D. Gall, A. Rockett, I. Petrov, J.E. Greene, Phys. Rev. Lett. 89 (2002) 176102.
[7] S. Kodambaka, V. Petrova, A. Vailionis, I. Petrov, J.E. Greene, Surf. Sci. 526 (2003) 85.
[8] S. Kodambaka, D.L. Chopp, I. Petrov, J.E. Greene, Surf. Sci. 540 (2003) L611.
[9] K. Morgenstern, G. Rosenfeld, G. Comsa, Phys. Rev. Lett. 76 (1996) 2113.
[10] K. Morgenstern, G. Rosenfeld, G. Comsa, Surf. Sci. 441 (1999) 289.
[11] G.S. Icking-Konert, M. Geisen, H. Ibach, Surf. Sci. 398 (1998) 37.
[12] J.B. Hannon, C. Klünker, M. Giesen, H. Ibach, N.C. Bartelt, J.C. Hamilton, Phys. Rev. Lett. 79 (1997) 2506.
[13] N.C. Bartelt, W. Theis, R.M. Tromp, Phys. Rev., B 54 (1996) 11741.
[14] M. Li, J.F. Wendelken, B.-G. Liu, E.G. Wang, Z. Zhang, Phys. Rev. Lett. 86 (2001) 2345.
[15] M. Giesen, G. Schulze Icking-Konert, H. Ibach, Phys. Rev. Lett. 80 (1998) 552.
[16] M. Giesen, G. Schulze Icking-Konert, H. Ibach, Phys. Rev. Lett. 82 (1999) 3101.
[17] K. Morgenstern, G. Rosenfeld, G. Comsa, M.R. Sørensen, B. Hammer, E. Lægsgaard, F. Besenbacher, Phys. Rev., B 63 (2001) 045412.
[18] M.J. Rost, R. van Gastel, J.W.M. Frenken, Phys. Rev. Lett. 84 (2000) 1966.
[19] M.J. Rost, S.B. van Albada, J.W.M. Frenken, Phys. Rev. Lett. 86 (2001) 5938.
[20] M.J. Rost, S.B. van Aldaba, J.W.M. Frenken, Surf. Sci. 515 (2002) 344.
[21] M.J. Rost, S.B. van Aldaba, J.W.M. Frenken, Surf. Sci. 518 (2002) 21.
[22] K. Morgenstern, E. Lægsgaard, I. Stensgaard, F. Besenbacher, Phys. Rev. Lett. 83 (1999) 1613.
[23] S. Rusponi, C. Boragno, R. Ferrando, F. Hontinfinde, U. Valbusa, Surf. Sci. 440 (1999) 451.
[24] Y. Yao, Ph. Ebert, M. Li, Z. Zhang, E.G. Wang, Phys. Rev., B 66 (2002) 41407.
[25] W.W. Pai, N.C. Bartelt, J.E. Reutt-Robey, Phys. Rev., B 53 (1996) 15991.
[26] J.G. McLean, B. Krishnamachari, D.R. Peale, E. Chason, J.P. Sethna, B.H. Cooper, Phys. Rev., B 55 (1997) 1811.
[27] E. Bauer, Rep. Prog. Phys. 57 (1994) 895.
[28] S.V. Khare, T.L. Einstein, Phys. Rev., B 54 (1996) 11752.
[29] W.W. Pai, J.F. Wendelken, C.R. Stoldt, P.A. Thiel, J.W. Evans, D.J. Liu, Phys. Rev. Lett. 86 (2001) 3088.
[30] D.J. Liu, J.W. Evans, Phys. Rev., B 66 (2002) 165407.
[31] This approximation is valid when $(\tilde{\beta}(\varphi)\kappa(\theta)\Omega/kT)\ll1$. In the experiments reported in this paper, $(\tilde{\beta}(\varphi)\kappa(\theta)\Omega/kT)\leq0.01$ at $T\geq1550$ K [37].
[32] S.V. Khare, S. Kodambaka, D.D. Johnson, I. Petrov, J.E. Greene, Surf. Sci. 522 (2003) 75.
[33] I. Petrov, F. Adibi, J.E. Greene, W.D. Sproul, W.-D. Münz, J. Vac. Sci. Technol., A 10 (1992) 3283.
[34] R.M. Tromp, M.C. Reuter, Ultramicroscopy 36 (1991) 99.
[35] Inorganic Index to Powder Diffraction File (Joint Committee on Powder Diffraction Standards, Pennsylvania, 1997). Card numbers 38-1420 and 08-0117 for TiN and TiO, respectively.

[36] Image SXM, developed by Prof. Steve Barrett, Surface Science Research Centre, Liverpool, England, 2002 (http://reg.ssci.liv.ac.uk).
[37] S. Kodambaka, Navot Israeli, J. Bareño, W. Święch, Kenji Ohmori, I. Petrov, J.E. Greene, Surf. Sci. 560 (2004) 53.
[38] The [111] direction in NaCl-structure TiN is polar, consisting of alternating layers of Ti and N atoms.
[39] S. Kodambaka, V. Petrova, A. Vailionis, P. Desjardins, D.G. Cahill, I. Petrov, J.E. Greene, Thin Solid Films 392 (2001) 164.
[40] This result is higher than the corresponding value 0.73 ± 0.04 obtained at lower temperatures (1050–1250 K) [3,6], consistent with the expected decrease in step energy anisotropy with temperature.
[41] A. Emundts, M. Nowicki, H.P. Bonzel, Surf. Sci. 496 (2002) L35.
[42] M. Nowicki, A. Emundts, H.P. Bonzel, Prog. Surf. Sci. 74 (2003) 123.
[43] The lattice constant of NaCl-structure TiN is $a = 4.24$ Å [35]. The intersection between the unit cell and the (111) plane that crosses its center is an equilateral triangle of side $a\sqrt{2}$. It contains 2 TiN units in an area of 15.6 Å^2, thus $\Omega = 7.8$ Å^2.